The 2-μm spectroscopy of Huygens probe landing site on Titan with Very Large Telescope/Nasmyth Adaptive Optics System Near-Infrared Imager and Spectrograph

A. Negrão, M. Hirtzig, A. Coustenis, E. Gendron, P. Drossart, Pascal Rannou, M. Combes, Vincent Boudon

The 2-μm spectroscopy of Huygens probe landing site on Titan with Very Large Telescope/Nasmyth Adaptive Optics System Near-Infrared Imager and Spectrograph

A. Negrão,[1,2,3] M. Hirtzig,[1,4] A. Coustenis,[1] E. Gendron,[1] P. Drossart,[1] P. Rannou,[3] M. Combes,[1] and V. Boudon[5]

Received 25 November 2005; revised 26 July 2006; accepted 4 October 2006; published 16 February 2007.

[1] Several ground-based telescopes followed the event of the Huygens probe descent through Titan's atmosphere (14 January 2005). We used the Nasmyth Adaptive Optics System Near-Infrared Imager and Spectrograph (NACO) adaptive optics system at the UT-4 of the Very Large Telescope in Chile to perform both spectroscopic and imaging measurements of Titan. We present here a selected sample of the spectra we acquired on 16 January 2005 in the K band between 2.03 and 2.40 μm. Our spectra include the Huygens landing site and surrounding dark and bright areas. We apply a radiative transfer code using new methane absorption coefficients calculated in the 2-μm region. The analysis of the data yields information on the atmosphere and surface properties of these areas. The latter seem to indicate a strong decrease of Titan's surface albedo between 2.03 and 2.12 μm in all areas. This is compatible with the presence of ices such as CH_4 and H_2O at the surface. Sensitivity tests on the influence of the haze profile and the methane absorption on these results were performed.

Citation: Negrão, A., M. Hirtzig, A. Coustenis, E. Gendron, P. Drossart, P. Rannou, M. Combes, and V. Boudon (2007), The 2-μm spectroscopy of Huygens probe landing site on Titan with Very Large Telescope/Nasmyth Adaptive Optics System Near-Infrared Imager and Spectrograph, *J. Geophys. Res.*, *112*, E02S92, doi:10.1029/2005JE002651.

1. Introduction

[2] Saturn's largest moon, Titan, is a unique world and the only other object in our Solar system to possess a substantial atmosphere of nitrogen, like our own planet. For this and other reasons it has attracted the interest of the astronomical community for several centuries since its discovery by Christiaan Huygens in 1655, and became a privileged target of the recent Cassini-Huygens mission to the Saturnian system.

[3] In the past, Titan has been extensively studied remotely from the Earth and space (Voyager, ISO, Hubble Space Telescope). For the ground-based or near-Earth observations, three techniques have been applied: radar, spectroscopy and imaging measurements. On 14 January 2005, after a successful separation from the mother spacecraft, Cassini, the Huygens probe entered Titan's atmosphere, performed a multi-instrumental investigation during a 2.5 hour descent, and landed on Titan's surface, where it continued to return data for several more minutes. During the Huygens descent, observations were performed from several large telescopes in order to record/monitor and to follow the event. We report here on data that are part of an observational campaign conducted on 15 and 16 January at the Very Large Telescope (VLT) in Chile, with the Nasmyth Adaptive Optics System Near-Infrared Imager and Spectrograph (NAOS/CONICA) adaptive optics system installed at the Nasmyth focus of the 8.2-m mirrored UT-4 "Yepun" telescope of the VLT [*Rousset et al.*, 2003]. The infrared camera CONICA is sensitive in the 0.9–5 μm, but like our previous runs on this instrument [see, e.g., *Gendron et al.*, 2004] we focused, during this campaign, on the 1–2 μm domain, choosing in this paper to study only 16 January data of the 2-μm methane window. The other spectral regions recorded in this run are discussed by *Hirtzig et al.* [2006, 2007].

2. Observations

[4] Adaptive optics allows compensation in real-time for the wavefront distortions induced by the turbulence of Earth's atmosphere. This effect, responsible for the degradation of the spatial resolution of any ground-based observation, is cancelled, and the image quality is thus restored as if the telescope was in space. It is a powerful tool commonly adopted today in the study of solar system objects, and it has been frequently applied for the past 10 years to Titan.

[1] Laboratoire d'Etudes Spatiales et d'Instrumentation en Astrophysique, Observatoire de Paris-Meudon, Meudon, France.
[2] Observatório Astronómico de Lisboa, Lisbon, Portugal.
[3] Service d'Aéronomie, Institut Pierre Simon Laplace, Université de Versailles Saint-Quentin-en-Yvelines, Verrières le Buisson, France.
[4] Laboratoire de Planétologie et Géodynamique, Nantes, France.
[5] Laboratoire de Physique de l'Université de Bourgogne, Dijon, France.

0148-0227/07/2005JE002651

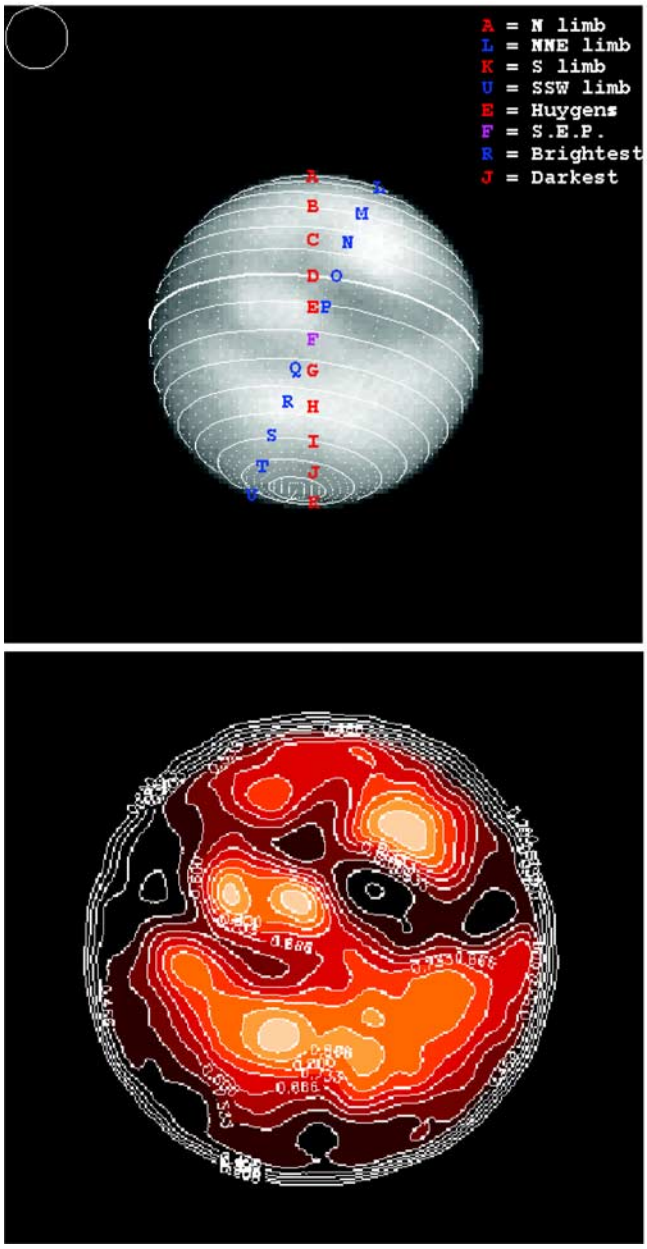

Figure 1. (top) NAOS/CONICA image with the 21 pixels from 16 January 2005, along two slits, one vertical and one diagonal. The Titan spectra were acquired in the K band with the S27_3_SK mode and labeled A to U. We focus here on only three of them: D, which corresponds to a dark area; R, which corresponds the brightest region observed; and E, which concerns the Huygens landing site. (bottom) The same image in color and with isocontours highlighting the Titan normalized surface albedos at 2.03 μm. The brightest area is set to 1.

The succession of methane absorption bands and windows in the near-infrared allows astronomers to study the atmospheric and surface properties [*Griffith et al.*, 1991; *Coustenis et al.*, 1995]. Besides the recent advances achieved in Titan's near-infrared spectroscopy from Earth and Earth-bound observatories such as ISO [e.g., *Griffith et al.*, 2003; *Lellouch et al.*, 2004; *Coustenis et al.*, 2006; *Negrão et al.*, 2006], imaging has also played an important part in unveiling some of Titan's mysteries [*Smith et al.*, 1996; *Coustenis et al.*, 2001; *Roe et al.*, 2002; *Hirtzig et al.*, 2006]. A combination of these two approaches is an optimal way to investigate Titan's lower atmosphere and surface [*Brown et al.*, 2002].

[5] In this study we present Titan data taken on 16 January 2005, with NACO in the K band (from 2.03 to 2.40 μm) which includes part of the 2.0-μm methane window and also the nearby methane band. For a complementary discussion about the observation techniques and the analysis of these data and also of those taken on 15 January with the same instrument, see also *Hirtzig et al.* [2006, 2007]. The spectral resolving power of the S27_3_SK grism was about 700, and the spatial resolution along the NACO slit was about 0.08 arc sec. Since Titan's size was 0.88 arc sec, we recovered 11 spectra along one diameter of Titan, spanning nearly 500 km at the center of the disk. Two series of spectra were acquired, overlapping on the sub-Earth point, allowing us to harvest 21 spectra along two diameters on Titan's disk (Figure 1, top). We selected three spectra for analysis: (1) the spectrum associated with the pixel located exactly on the Huygens landing position (12°S, 194°W); (2) the spectrum of a dark area on this image (0°N, 195°W); and (3) the spectrum of the brightest area on this same image (47°S, 200°W). Figure 1 (bottom) shows, for 2.03 μm, the albedo (in arbitrary and normalized units) isocontours of the image in Figure 1 (top). Here the R (brightest) region has a normalized albedo of 1, D (the dark area) has, with respect to R, an albedo of 0.6, that is 40% lower than the brightest region, and E (the Huygens' landing site) has, always with respect to R, an albedo between 0.6 and 0.8 (difficult to restrict because of the large intensity gradient in this region caused by the proximity of the F bright area and the D dark zone).

[6] Our aim is to infer information on the surface albedo of these three regions and to characterize the Huygens landing site with respect to surrounding surface terrains. For this purpose, we need to constrain atmospheric properties such as the haze and the methane abundance. Therefore, for each spectrum, we fit the data in the methane band (longward of 2.12 μm) by adjusting the model parameters related to the description of the atmosphere: aerosol concentration, cutoff level of their vertical distribution, methane abundance, and so on. When this adjustment is done, we apply directly the returned atmospheric parameters into the inversion procedure of the model, retrieving the surface albedo from the intensity, given the characteristics of the atmosphere above each location.

2.1. Data Processing

[7] Two series of spectra were acquired, along two diameters of the satellite, as shown in Figure 1 (top). The size of the spatial resolution element is given by the contour of the black disk in the top left corner of Figure 1 (top). This is about 5 times coarser than the resolution of the camera used here. Thus each spectrum we show is the weighted sum of 5 contiguous pixels on the CCD. We limited the analysis to the spectral range of 2.03–2.40 μm, thus avoiding problems with the very low signal longward of 2.40 μm, and in particular the risk of divergence when trying to correct for the terrestrial absorption features.

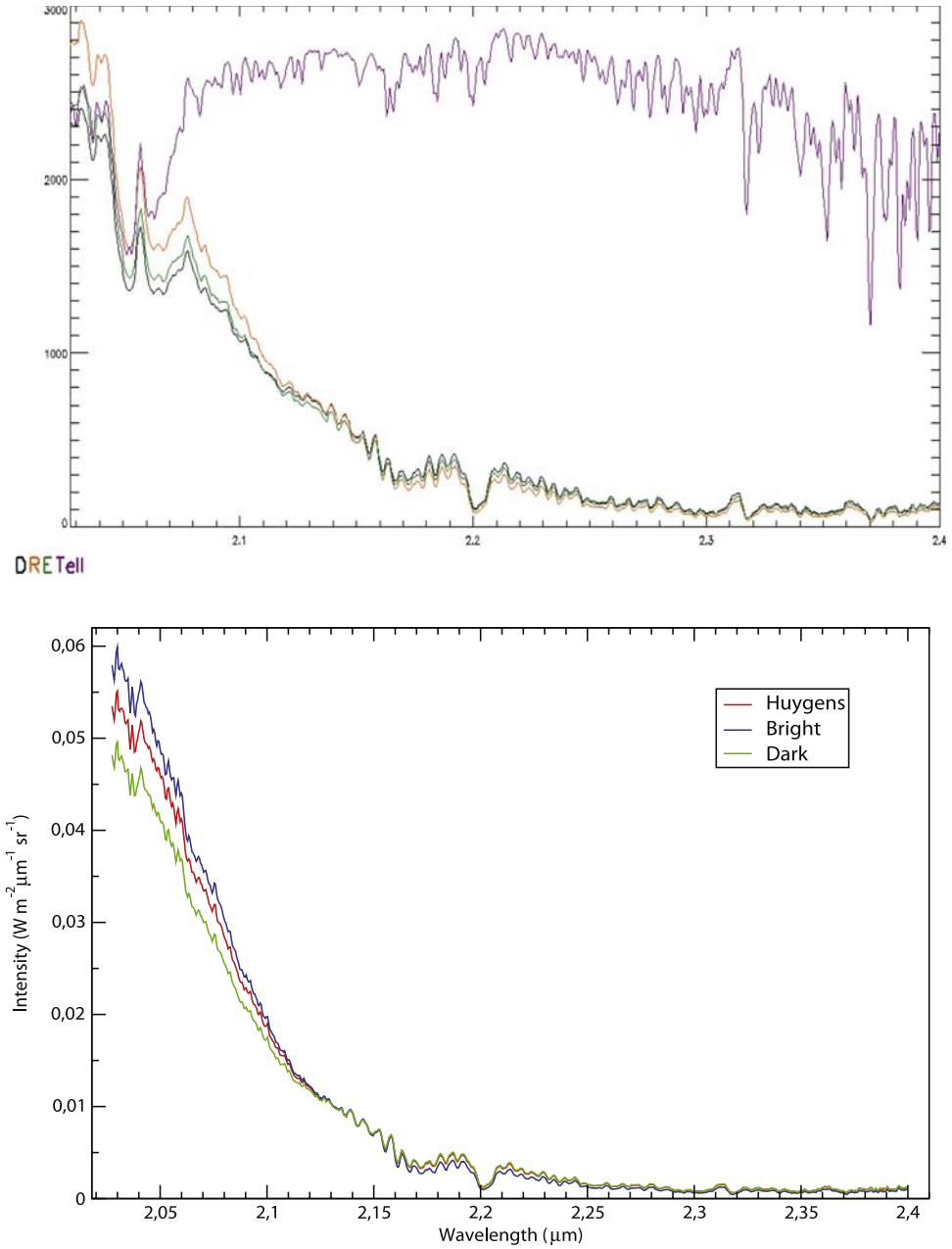

Figure 2. (top) Raw spectra (analog-to-digital unit versus wavelength) of the three regions (E in green, R in gold, D in black), with the spectrum of a standard photometric star (in violet, fitted to the telluric features on the Huygens landing site) to help us correct for the terrestrial atmospheric absorption features (mainly shortward of 2.1 and longward of 2.3 μm). (bottom) Calibrated spectra in W m^{-2} μm^{-1} sr^{-1} of the three regions of interest here. We use the data in the methane band, longward of 2.12 μm, to fix the atmospheric parameters. As a second step, with the atmospheric profile fixed, we let the surface albedo be the only variable parameter to fit in the methane window.

[8] The reduction of the spectrograms saved as regular CCD images, involves flat-fielding, bad pixels removal and correlated noise correction (as in previous works, e.g., *Coustenis et al.* [2005]). Figure 2 (top) displays the raw spectra of the R, E and D locations along with the raw spectrum of a standard star (HD104076), exhibiting the deep absorption bands due to the Earth's atmosphere (especially shortward of 2.1 μm and longward of 2.3 μm).

2.2. Flux Calibration and Correction for Telluric Features

[9] During our observing night, we acquired the spectrum of a G0V standard star (Hip058454 or HD104076; mag$_K$ = 7.17: *Perryman et al.* [1997]), displayed in violet in Figure 2 (top). We used this spectrum to calibrate our spectra in flux. This star was chosen so as to be close to Titan's position at the time of the observations, thus with a similar Earth air

mass value (Titan = 1.68, star = 1.90). After the flux calibration the spectra show values around 10^{-3} to 10^{-4} W m^{-2} μm^{-1} sr^{-1} in the methane band. These values are compatible with the Visual and Infrared Mapping Spectrometer (VIMS) measurements [*Barnes et al.*, 2005].

[10] The calibrated spectra for the bright, dark, and Huygens landing site areas (letters R, D, and E in Figure 1 (top), respectively) are shown in Figure 2 (bottom). In the CH_4 band, longward of 2.2 μm, the data of the D and E locations are very similar, implying compatible atmospheric compositions at high altitudes. Between 2.12 and 2.2 μm we sound lower altitudes (see section 4.1.1), more sensitive to the atmospheric composition near the ground. Finally, shortward of 2.12 μm, the data are sensitive to the surface albedo.

[11] In Figure 1 (top) the labels highlight the different areas covered during our campaign where we have recorded spectra of Titan's disk, illustrated here on a nondeconvolved NB_2.00 image. Note that in this study, while we have the spectrum of one of the brightest regions available on this image (location R), we have not been able to acquire the one of the darkest area (located to the right of the P pixel, Figure 1 (top)). Therefore we limit our ''dark area'' studies to a dark region on the equator (location D). These two regions furthermore satisfy the conditions of being close to (1) the landing site of Huygens (locus E) and (2) the center of the disk. This latter criterion is a precaution to dampen the overcorrection or undercorrection artifacts possible when choosing locations with different air masses or viewing geometries, even though such parameters are taken into account in our radiative transfer model.

3. Radiative Transfer Model

[12] To retrieve the atmospheric and surface properties of Titan, we applied the microphysical and radiative transfer model of *Rannou et al.* [2003] to the data. This is a one-dimensional (1-D) plane-parallel model with 70 layers from the ground up to 700 km. Each layer is 9.4 km deep, except the highest one that is 50 km high. The temperature and pressure profiles used are from *Lellouch et al.* [1989] and *Lellouch* [1990]. The radiative transfer part of the code is basically the *McKay et al.* [1989] code. The additional microphysical part of the model, which deals with the growth and optical properties of aerosols, is described by *Rannou et al.* [2003]. It calculates the haze opacity, the haze single scattering albedo and the haze asymmetry factor, which are required in the radiative transfer calculations. The haze single scattering albedo ranges, all wavelengths considered, from about 0.3 to about 0.97 from 400 km down to 200 km in altitude below which level it maintains this last value. The haze asymmetry factor ranges from about 0 to about 0.44 from 400 km down to 100 km in altitude. Below this level it maintains the constant value of 0.44.

[13] The aerosols distribution (which in this version of the code are fractally shaped) depends on the haze production rate, the haze production pressure, the aerosol charging rate and the eddy diffusion coefficient. The values assumed for these variables follow from *Rannou et al.* [2003] and are defined as 0.805×10^{-13} kg m^{-2} s^{-1}, 1.5 Pa, 20 e^- μm^{-1} and 0, respectively.

[14] Other important inputs are the aerosol imaginary refractive index, the methane vertical profile, the methane absorption coefficients and the ground reflectivity. Although extensive laboratory work is performed nowadays on the production and optical properties of aerosols (see *Imanaka et al.* [2004] for a recent review), the *Khare et al.* [1984] imaginary refractive index measurements are still the most widely used and with a larger spectral coverage. We include these in this work.

[15] The methane opacity (the most important opacity source in Titan's near-infrared) is obtained from the methane abundance and from its absorption coefficients. The methane mixing ratio, as a function of altitude, follows a simple behavior in this 1-D model. It is defined at the surface, remains constant in altitude until the saturation point, follows the saturation curve up to the tropopause, and finally remains constant above that level. This behavior with altitude is based on the one obtained by *Lellouch et al.* [1989].

[16] A good choice of the methane absorption coefficients is very important since they have a major impact on the modeling in the near-infrared part of the spectrum. In this work we use the methane absorption coefficients based on the work of *Hilico et al.* [1994] and subsequent improvements included in the Spherical Top Data System database [*Wenger and Champion*, 1998] (see also at http://www.u-bourgogne.fr/LPUB/TSM/sTDS.html for latest updates). This database is built from a theoretical model of the methane rotation-vibration interactions and transition moments whose molecular parameters (Hamiltonean and dipole moment) were calibrated in frequency and intensity against laboratory high-resolution absorption spectra obtained at different temperatures (between 80 and 300 K) and different pressures. It can be summarized as follows:

[17] 1. High-resolution (with a spectral resolution of 0.001 cm^{-1}) spectra are recorded using Fourier transform (FTIR) spectroscopy. These data are completed by complimentary techniques like stimulated Raman and microwave spectroscopy which give access to additional data.

[18] 2. These spectra are assigned and the line positions are used to fit effective Hamiltonian parameters. At this stage, a ''primitive'' dipole moment model is used to calculate rough intensities. Using these results, a first prediction is derived.

[19] 3. In each spectral region, several new high-resolution FTIR spectra are recorded at different temperatures and pressures. A multispectrum fit is performed to determine precise line parameters (positions, intensities, widths). The first simulation is used to ''deconvolve'' the spectra because, in general, many lines are not isolated but are in fact superpositions of several transitions. An absolute intensity list is then produced for the standard temperature of 296 K.

[20] 4. This list is then finally used to fit the effective dipole moment parameters.

[21] Contrary to the extrapolation to high temperatures, which would involve more excited levels that have not been studied experimentally and thus would not be included in the fit, the extrapolation to the low temperatures of Titan is reasonably reliable since it does not involve new energy levels.

[22] A description of these coefficients is given by *Coustenis et al.* [2006], and for a more in-depth discussion of their calculation, see *Boudon et al.* [2006]. These

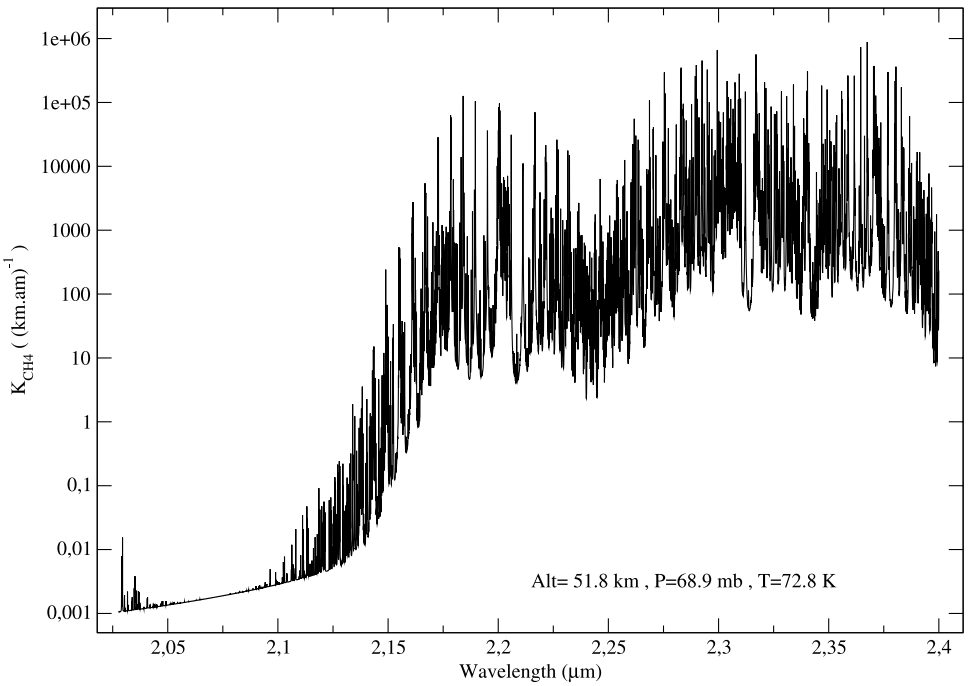

Figure 3. Example of the methane absorption coefficients used in the model. The ones shown were computed for a temperature of 72.8 K and a pressure of 68.9 mbar, which corresponds to an altitude of 51.8 km in Titan's atmosphere.

absorption coefficients were computed for each pressure and temperature layer of our model. In Figure 3 we show an example of one of these calculations, in this case for 51.8 km of altitude, where we have a temperature of 72.8 K and a pressure of 68.9 mbar. Thus our model benefits from this improved methane absorption description.

[23] Generally, the zenith-observer angle at each atmospheric layer along the line of sight depends on the altitude and this is more noticeable as we approach the limb. Although this is a 1-D plane-parallel model, this problem was taken into account by implementing a geometrical correction that enabled us to calculate the intensity at a certain distance from Titan's disk center (at points E, R, and D, as mentioned previously, Figure 1 (top)). The efficiency of this correction was tested against a 3-D spherical Monte Carlo model by *Tran and Rannou* [2004] and found to give an excellent agreement.

[24] A similar model was also used by *Gibbard et al.* [2004] to analyze speckle and adaptive optics images at the Keck telescope using the K′ broadband filter (1.96–2.92 μm). Their aim was to construct surface albedo maps at 2 μm and determine the haze optical depth at 2 μm at different solar longitudes. Their model is essentially the same as ours and also includes the geometrical correction mentioned previously. Main differences concern the number of layers and the methane absorption coefficients used. Their atmospheric grid consisted in only three layers so that they only retrieved the integrated haze opacity and not a complete vertical haze distribution. Nevertheless, the most important difference concerns the methane absorption treatment. While we use calculated values for the methane absorption coefficients in this work (the line-by-line calculations by *Boudon et al.* [2006]), *Gibbard et al.* [1999, 2004] assumed the methane to be completely absorbing within the fraction of the filter that it is in the methane band (59% for they K′ filter) and completely transparent outside of the methane absorption band. This method, while reasonably adequate to retrieve surface maps of Titan in the center of the methane windows (in the *Gibbard et al.* [2004] case, at 2 μm), is not sufficient to retrieve a surface spectrum all through the 2 μm methane window and wing.

4. Results of the Model

4.1. Atmospheric Properties

[25] The fits of the Huygens landing site spectrum, of the brightest area and of a dark region (regions E, R, and D in Figure 1 (top), respectively) are shown in Figures 4 (top), 4 (middle), and 4 (bottom). The calculations were performed with a spectral resolution of 0.1 cm^{-1} (the same as the resolution of the methane coefficients at our disposal) and then convolved to the same resolution as the data, R = 700 (6.5 cm^{-1} at 2.2 μm).

[26] Generally, 1-D models assume the same haze profile for all latitudes to calculate the geometric albedo of Titan's disk (with some exceptions, as, for instance, in the analysis of Hubble Space Telescope images by *Young et al.* [2002]). On the other hand it is well known that the haze distribution depends on latitude. Because our data are spatially resolved, we assumed the vertical haze profile to vary with latitude, so that we obtained a haze profile for each of the three locations of the three spectra previously described. We start from the nominal haze profile of *Rannou et al.* [2003] and adapt it to fit the different spectra, as explained in section 4.1.2.

[27] We assumed the same methane abundance at these three latitudes, namely, 5% at the surface in accordance with recent Huygens/Descent Imager/Spectral Radiometer

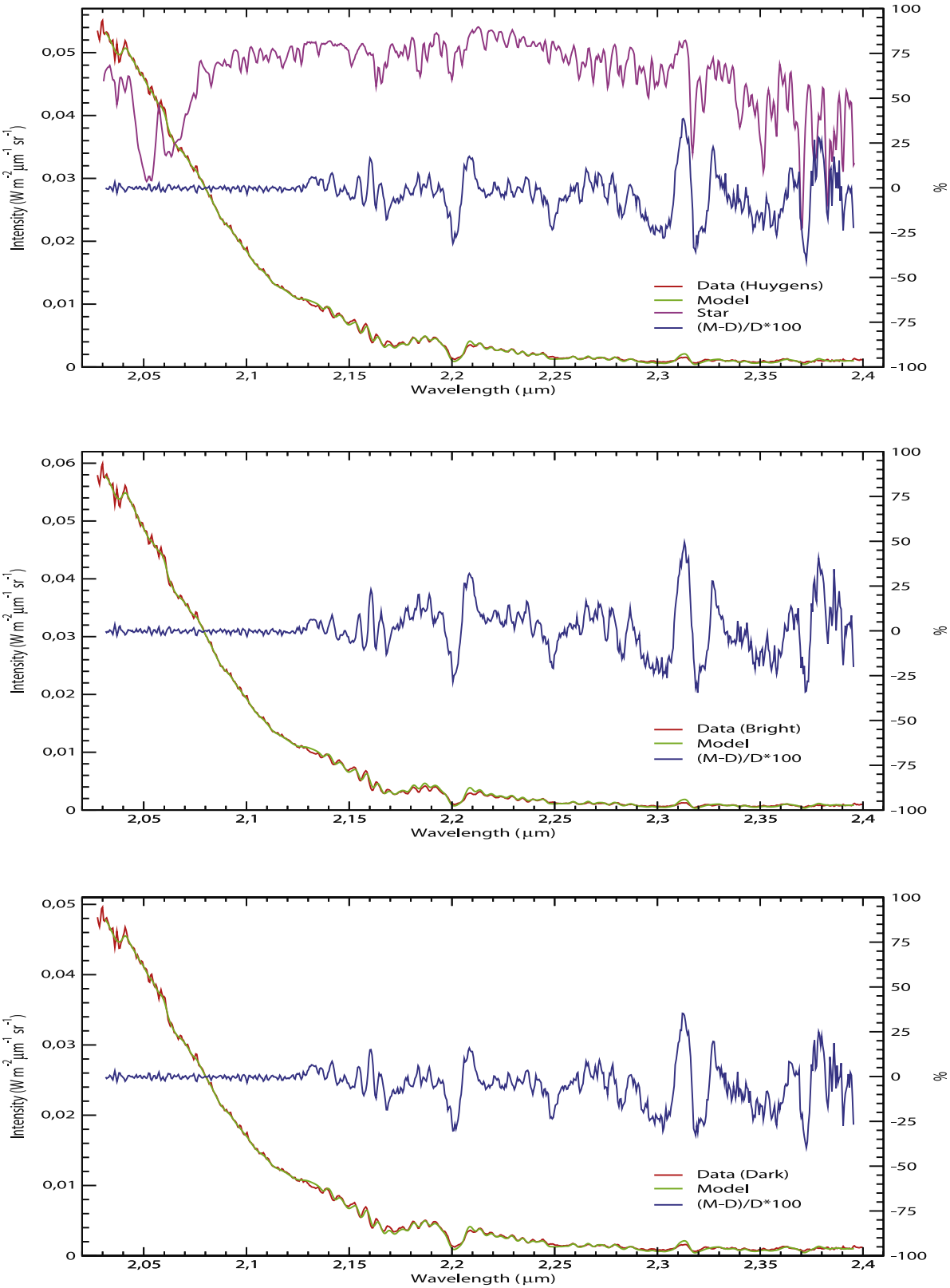

Figure 4. Fits to the spectra: best fit of (top) the Huygens landing site, (middle) the brightest site, and (bottom) the dark area right above the Huygens site. The error bars in these fits are about ±27% (3σ) beyond 2.12 μm and $^{+3}_{-12}$% (3σ) below 2.12 μm (see text for details). Also shown in plot is the difference, in percentage, between the data and the model. Because this last one is almost always less than 25%, our fits are good to within 3σ. In Figure 4 (top) are also shown, in violet, the star spectra in arbitrary units.

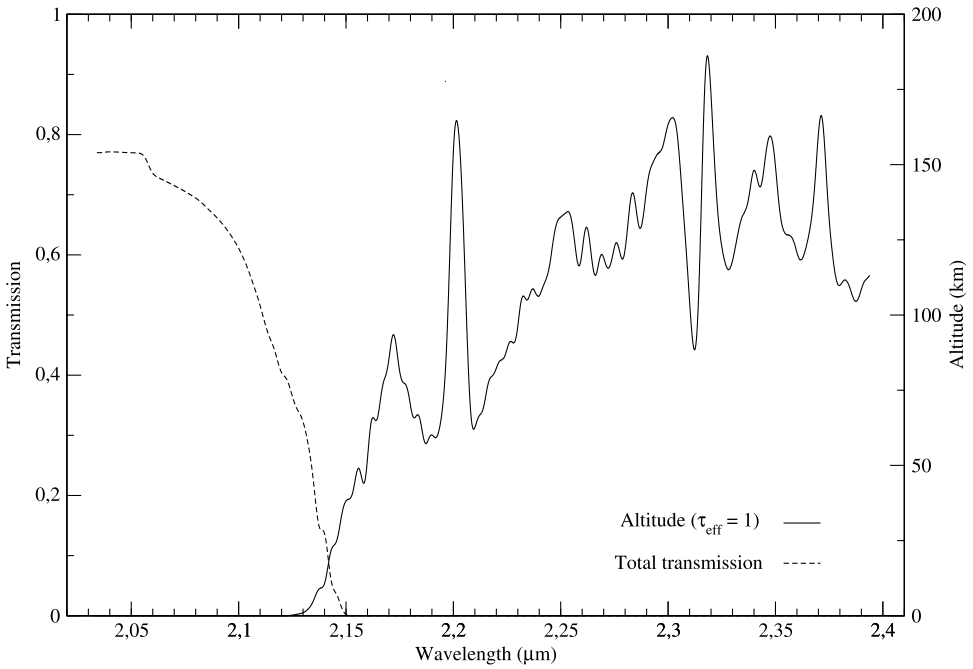

Figure 5. Altitude probed and total transmission (haze + gas) as a function of wavelength. The transmission of 0.8 near the center of the methane window is mainly due to the haze contribution to the total transmission (see text for details).

(DISR) results [*Tomasko et al.*, 2005], pertaining to location E in particular. With this abundance at the surface, the vertical profile of the methane mixing mole ratio is calculated as explained earlier and depends on the pressure and temperature at each layer of the model. We find that the 5% mixing ratio value on the surface yields a stratospheric value of 1.7% and provides a good fit in the 2.12–2.2 μm range, the spectral region most sensitive to the methane abundance in the lower troposphere for all sites.

[28] Figure 4 displays the model fits of our data and for clarity purposes shows the difference, in percentage, between the data and the model. The three areas where the fits are the worst are located at 2.2, 2.32 and 2.37 μm in the strong methane features. The discrepancies between the model and the data we find in these areas could be explained in part by the methane absorption coefficients used in this work. Indeed, the *Boudon et al.* [2006] analysis is lacking in line shapes and is perfectible in line positions and intensities in the 2-μm region, the spectral region studied here. The error on the calculation of the geometric albedo with our model, taking into account the uncertainty due to the data, the haze and the methane absorption coefficients, was found to be about ±27% (3σ) beyond 2.12 μm mainly due to a haze extinction variation of 10%, and $^{+3}_{-12}$% (3 σ) below 2.12 μm mainly due to the data noise level. Hence our fits are good to within 3σ since the difference between the model and the data is almost always less than 25% (see Figure 4).

4.1.1. Atmospheric Transmission and Altitudes Probed

[29] Titan's atmospheric methane is the main absorber in the near-infrared and thus the most influent parameter in defining the altitudes probed in this spectral region. Although not as strongly as for the visible, haze also contributes to the total opacity in the near-infrared but, in this last case, at a much lower level than methane. Figure 5 plots a curve of the altitude probed as a function of wavelength. This altitude refers to the level where the total effective opacity is equal to 1. The effective opacity, defined by *Pollack and McKay* [1985] and also used by *Rannou et al.* [2003], is defined as $\tau_{eff} = \tau \times \sqrt{(1-w) \times (1-w \times g)}$, where τ is the total opacity (haze + gas), w is the total single scattering albedo (average of the single scattering albedo of haze and gas), and g is the total asymmetry factor (average of the asymmetry factor of haze and gas). Both the total single scattering albedo and the total asymmetry factor depend on the wavelength and altitude. The total single scattering albedo ranges from 0 to 0.97, and the total asymmetry factor ranges from 0 to 0.47, all wavelengths and altitudes considered. The effective opacity definition takes into account the photons that are scattered forward by the haze particles and so are not lost to the downward flux. This correction tends to be more important as we approach the visible part of the spectrum, while negligible near the longer-wavelength part of the near-infrared.

[30] In Figure 5 we plotted a curve of total transmission (haze + gas) as a function of wavelength. Although the transmission due only to methane in the 2-μm window is nearly 1, haze also contributes to the total opacity as mentioned above. As shown in Figure 5 (and also by *Negrão et al.* [2006, Figure 7a], who show a curve of the haze transmission from 0.9 to 2.5 μm), the transmission due only to the haze in this spectral region is around 0.8. Thus, although the haze extinction generally decreases with increasing wavelength in the infrared region, it still has an important contribution to the total opacity at 2 μm and masks in part this methane window. Therefore, at the center of the 2-μm window, the atmosphere is not completely transparent, as would be the case in the ideal situation of an

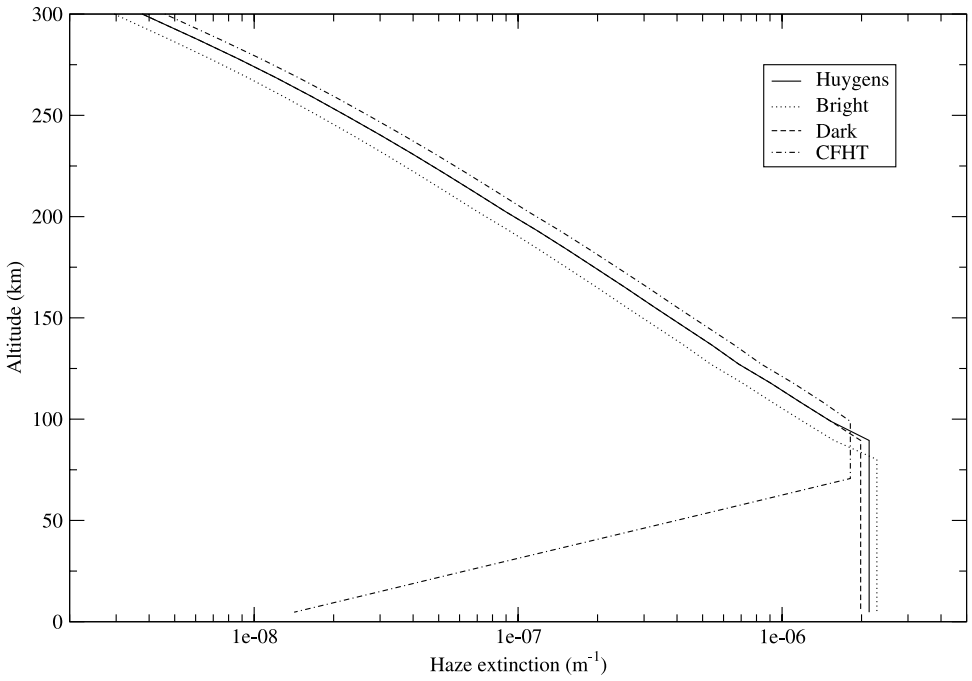

Figure 6. Haze extinction at 2.04 μm for each of the three areas studied in this work. The Huygens landing site and the dark region have similar atmospheric haze contents in the upper atmosphere, above roughly 90 km, below which level they differ, with the dark region showing a slightly smaller haze extinction at lower altitudes. This small difference is introduced to optimize the fits in the methane band wings of the Huygens landing site and dark regions. The bright region requires a smaller haze concentration at high altitudes in order to account for the lower intensity value in the methane band, longward of 2.2 μm. Also shown is the haze profile used by *Negrão et al.* [2006] for the analysis of CFHT data. This latter profile has a quite different behavior below 110 km in altitude with a radical reduction of the aerosol content.

atmosphere composed only of methane. In reality there is also the contribution of the scattered (by the haze) light to the total observed flux. This scattered light blurs Titan's surface images taken in the methane windows and in particular as we approach the visible regions of the spectrum. This highlights the need for modeling Titan's atmosphere and the simulation of the light interaction with Titan's aerosols in particular (even if we observe in a methane window), in order to retrieve information about Titan's surface. The contribution of the scattered light by the haze is thus taken into account by our model in the total flux and, consequently, also in the retrieval of the surface albedo in this methane window.

4.1.2. Haze Profile

[31] Using the altitude curve as an indication for the atmospheric levels probed allows us to invert the haze vertical profile. To a given spectral interval, we associate a certain altitude interval, which can thus be used to constrain the haze at that level. The intensity will evidently depend on the haze found at the probed altitude but also at higher levels. A similar procedure to this one was used by *Ádámkovics et al.* [2006]. The inversion of the haze will thus naturally start from the highest levels, that is to say, by fitting first the region roughly from 2.2 to 2.4 μm (Figure 5). Figure 2 (bottom) shows that in this spectral region, the data at the E and D locations are very similar, thus indicating a similar higher atmospheric haze profile. This is not surprising since their projections on Titan's disk are not very distant. The fit of the E and D regions resulted indeed in an equal haze vertical profile, above 90 km, for the two spectra (Figure 6). Nevertheless, the nominal vertical haze profile, as predicted by the microphysical part of the model and used as an initial attempt to fit the data, did not exactly fit the intensity longward of 2.2 μm for the E and D locations. It yielded values somewhat lower than the observed ones thus indicating a lack of scatterers at high altitudes. An increase of 15% in the concentration (for both E and D locations) of the nominal haze profile was thus applied to account for this difference.

[32] On the other hand, data from the R location, the brightest one, show lower intensity values than the E and D areas for the same spectral region, i.e., for λ higher than 2.2 μm (Figure 2, bottom). This indicates a smaller concentration of haze particles at high altitudes and at the latitude of the R location with respect to the E and D areas. In this case our nominal haze profile predicted intensity values somewhat higher than the observations. A decrease of 10% in the haze concentration was applied to the nominal haze profile to fit this region. These adjustments of the haze concentration are not surprising since we use a simple 1-D model that assumes a disk-averaged haze description, although it is well known that Titan's haze is not uniform all over the disk. We should note however that, on a disk-averaged basis, the model provides a good prediction of the Titan's haze profile longward of 2.2 μm.

[33] The next step is to fit the region situated roughly between 2.12 and 2.2 μm (see Figures 2, bottom, and 5). Having fixed the methane abundance as explained earlier, the haze profile in the lower part of the atmosphere could now be inverted. For all three locations, in this spectral range, the nominal model predicts intensity values higher than the observations. This indicates, as suggested previously by different authors [e.g., *Lemmon et al.*, 1995; *Rannou et al.*, 2003; *Chanover et al.*, 2003], a decrease of scattering particles (haze) near the ground. This could be due to methane condensation with the haze particles acting as condensation nuclei for the gas. We simulate this reduction by imposing a constant haze profile below an altitude that depends on the location of study. This was found to be 87 km for the Huygens landing site, 90 km for the dark location and 76 km for the brightest one. This aerosol reduction is not unique: various shapes of the vertical profile in the lower altitudes can produce similar fits. The important point is the need for the same integrated haze reduction (as predicted by the nominal model) to be applied at lower altitudes.

[34] The need for the corrections in the nominal haze output of the model does not obviate the use of the microphysical model (which calculates other optical properties such as the phase function and the single scattering albedo) but highlights the importance of dynamical effects (e.g., global Hadley cells, convection in the troposphere, dissipation near the surface or zonal and tidal winds) in Titan's haze distribution, which cannot be taken into account in this 1-D model. It is important to bear in mind that (1) a unique haze vertical profile cannot fit the three spectra simultaneously longward of 2.12 μm and (2) a haze decrease in the nominal haze vertical profile, as predicted by 1-D models, is needed at lower altitudes.

[35] Furthermore, it should be noted that other types of vertical haze reduction completely different in shape (such as for instance the one we used in our own study of the Canada-France-Hawaii Telescope (CFHT) Titan data [*Negrão et al.*, 2006]) predict a more dramatic decrease of the aerosol content in the lower atmosphere (see Figure 6). Although that haze profile produced a good fit of the CFHT data in several spectral regions and for different years (from 1993 to 1996), it does not provide an acceptable fit of our VLT data, especially in the 2.12 and 2.2 μm region. We perform hereafter a sensitivity test of this difference in the haze vertical distribution on our results.

[36] *Gibbard et al.* [2004] have calculated the 2-μm haze optical depth over the span of 1996–2004. In this time interval the solar longitude of Titan as varied from about 190° to about 290°. Gibbard et al.'s Figure 2 shows, at the top, the variation of the haze optical depth in the equatorial region as a function of the solar longitude. It falls from 0.18 to 0.12 between 1996 and 1997 and then increases up to 0.15 in 1998, remaining constant until 2003 (at Ls = 275°). In 2004 (at Ls $\sim$ 290°) their equatorial haze optical depth increased to 0.2. Although they used a broadband filter in their calculation of the haze optical depth, our 2.04 μm integrated haze optical depth can be used to complete their curve of haze optical depth versus solar longitude. Our integrated haze opacity at 2.04 μm yields a value of 0.264 for the Huygens landing site, 0.250 for the dark site (this one located at the equator) and 0.258 for the brightest one. The solar longitude at the time of Huygens landing was around 302°. The value of the haze optical depth obtained here for the equator (D region in Figure 1 (top)) is thus compatible with the increase of the equatorial haze optical depth between 2003 and 2004, as plotted on the top of Figure 2 of *Gibbard et al.* [2004]. In fact, the slope of the curve is about the same between 2003 and 2004 and (after we add our 0.25 value at Ls = 302°) between 2004 and 2005.

[37] A north-south asymmetry of the Titan albedo was observed by the Voyager spacecraft in the visible region of the spectrum, the southern hemisphere being brighter by about 20% than the northern one [*Smith et al.*, 1981, 1982; *Letourneur and Coustenis*, 1993]. This is related with haze seasonal variations in the stratosphere [*Sromovsky et al.*, 1981; *Lockwood et al.*, 1986] and is supposed to have a 30-year cycle. The first observational evidence for these seasonal changes was reported by *Caldwell et al.* [1992]. Later works [e.g., *Lorenz et al.*, 1997, 1999, 2001] reported also on north-south asymmetry observations and suggested a dependence on wavelength. The north-south asymmetry is more evident at blue wavelengths, weaker at ultraviolet and reverses at red and near-infrared wavelengths. This means that at the time of Voyager's encounters, the northern hemisphere should be brighter than the southern one at near-infrared wavelengths. Thus our results on the total haze opacity, taken together with the *Gibbard et al.* [2004] ones, bring one more confirmation of the present migration of the haze from the southern to northern latitudes (passing by the equator) since we are close to 30 years after the Voyager observations.

4.1.3. Methane Absorption Coefficients

[38] Besides studying the haze profile, we also tested in this work another set of methane absorption coefficients. It is the most recent published methane band model adapted to Titan's conditions, described in detail by *Irwin et al.* [2006]. Figure 7 shows the fits in the methane band (longward of 2.13 μm, where the VLT/NACO data features are only due to Titan's atmospheric methane), performed with the *Boudon et al.* [2006] methane absorption coefficients in green, and with the *Irwin et al.* [2006] methane absorption coefficients in blue. For a complete discussion about a comparative study of this and other band models and line-by-line calculations, see *Negrão et al.* [2006]. Because the band model coefficients have a maximum spectral resolution of 10 cm^{-1}, we convolved the observational data shown in Figure 7 and the fit obtained with the *Boudon et al.* [2006] absorption coefficients to this same spectral resolution. Although the line-by-line calculations seem to reproduce slightly better the observed gas features, ($\chi^2 = 1.34 \times 10^{-5}$ for the *Boudon et al.* [2006] coefficients versus $\chi^2 = 2.85 \times 10^{-5}$ for the *Irwin et al.* [2006] coefficients) we cannot infer any preference for a better performance among these two sets. The quality of the fits in both cases is very similar. Nevertheless, we slightly favor the use of the line-by-line methane absorption coefficients in this spectral region since these do not impose an upper limit to the spectral resolution at which the radiative transfer calculation is performed and therefore allow to better reproduce the small features found in the data, especially between 2.13 and 2.29 μm. The use of the two data sets allowed us to estimate the error due to the methane absorption coefficients parameter. This was taken into

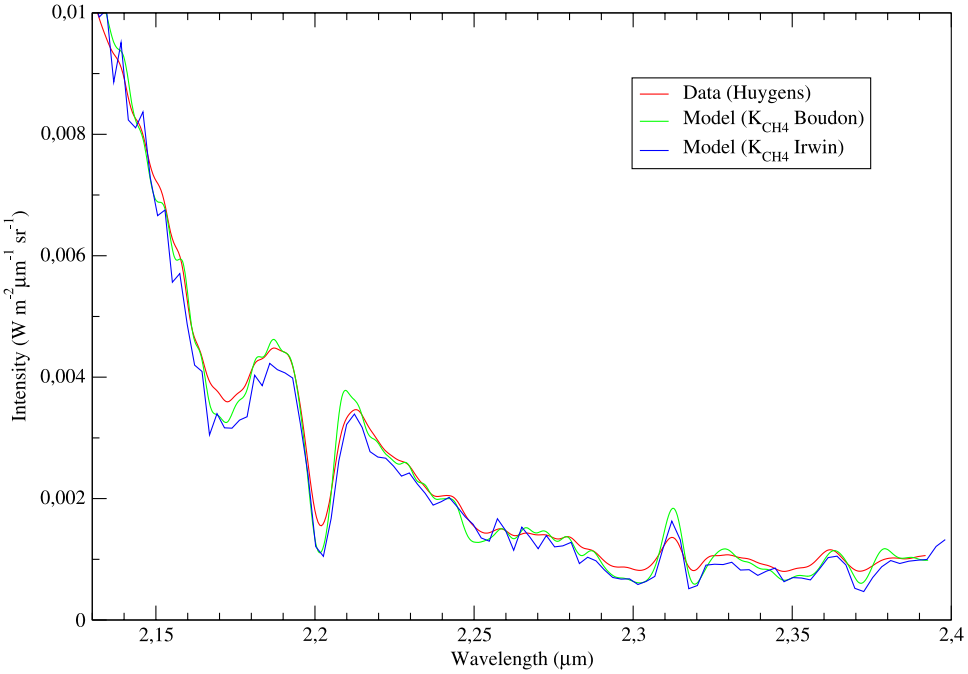

Figure 7. Fits to the data (in red) in the methane band, performed with the theoretical methane absorption coefficients of *Boudon et al.* [2006] (in green) and the band model coefficients of *Irwin et al.* [2006] (in blue), all of them at a spectral resolution of 10 cm^{-1}. Both the data and the fit performed with the *Boudon et al.* [2006] coefficients were convolved to the highest resolution available for the band model, 10 cm^{-1}. See text for details.

account in the calculation of the error associated to the retrieved intensity and surface albedo.

4.2. Titan's Surface

[39] Our data is sensitive to the surface reflectivity for wavelengths below 2.12 μm. Figure 5 shows that in this spectral region we probe the surface, although the total transmission is only around 0.8 in the center of the window. This is due to the haze contribution to the total transmission as discussed above.

[40] We fixed the atmospheric contribution for each of the three locations and inverted the surface albedo below 2.12 μm. The value of the total transmission shown in Figure 5 was taken into account in this inversion. Figure 8 shows the surface albedo obtained for the three regions: E (Huygens), R (Bright) and D (Dark) along with the error bars due to the haze, data and methane absorption uncertainties. Note that we do not have the whole methane window in our data. The center of the window is normally located at 2.03 μm [*Coustenis et al.*, 1995; *Griffith et al.*, 2003], and it extends from 2.0 to 2.06 μm. Although we normally attain the 2.03 μm in our spectral region, we may still be missing the real maximum albedo value for the 2-μm window, which could be higher, because we are at the border of our valid spectral region. With this caveat in mind, we find maximum values of 0.116 for the Huygens landing site, 0.108 for the dark area and 0.140 for the bright area.

[41] The error on the surface albedo retrieval naturally increases in the window wing. Sensitivity tests were performed by varying the total haze extinction by 10%. They result in a surface albedo uncertainty of 2.4% at 2.03 μm and up to 69% at 2.115 μm. The uncertainty from the data yields an error of 3.5% at 2.03 μm and up to 22% at 2.115 μm. The error due to the methane absorption coefficients is much smaller and equal to 1.1% at 2.03 μm and up to 4.3% at 2.115 μm. All these uncertainties taken together result in a total error of 4.9% at 2.03 μm rising to 74% at 2.115 μm. The absolute value of the total error is shown in the error bars of the surface albedo plotted in Figure 8.

[42] We performed another sensitivity test on the influence of the haze profile used in the retrieval of the surface albedo. We have made a calculation using the haze profile found from the analysis of our VLT data [*Negrão et al.*, 2006] and derived the associated surface albedo (as shown in Figure 8) with the associated uncertainties calculated as indicated above. Although the haze profile used by *Negrão et al.* [2006] does not provide the best possible fit to our data here in the methane band (see section 4.1.2) it still gives an acceptable match to the observations with a somewhat different surface albedo as a result. We thus find that the difference in haze profiles has a significant impact on the results. When we use the haze profile retrieved by *Negrão et al.* [2006], we find an increase in surface albedo of 4.9% at 2.03 μm and up to 130% at 2.115 μm.

[43] The variation of the surface albedo within this methane window as a whole from ground-based data has never been shown before *Negrão et al.* [2006] and this work. Prior to recent years and mainly due to the lack of appropriate methane absorption coefficients, only the albedos in the center of the methane windows were calculated. This new result can give additional constraints on the retrieval of the surface constituents. First in terms of spectral shape and then in terms of surface albedo values. Our

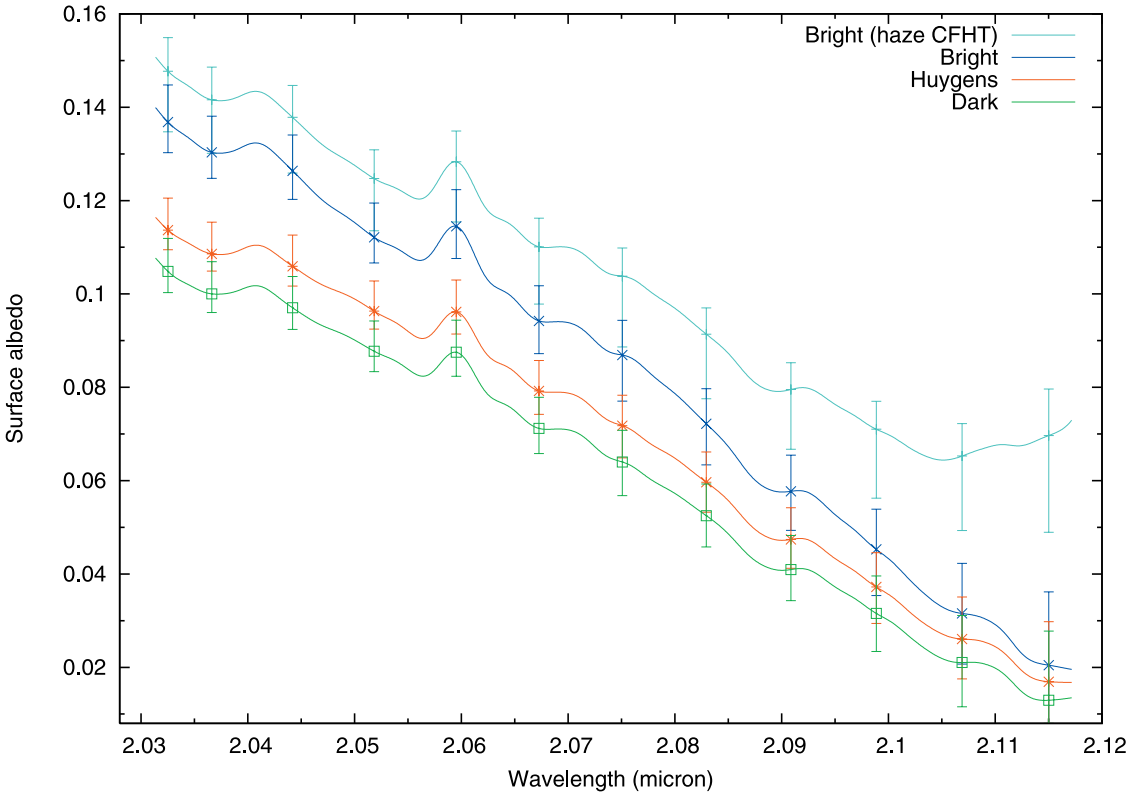

Figure 8. Surface albedo of the brightest area, of the dark area and of the Huygens landing site in the 2-μm methane window. Note that we do not have the whole window region in our data. The error bars due to the haze, data, and methane absorption uncertainties are also presented. We note the strong decrease of the surface albedo from the center of the window to its wing for all three locations. Also shown is the surface albedo that would have been obtained if the haze profile used for the analysis of the CFHT data (see Figure 6) was applied in our calculations. See text for more details.

retrieved surface albedo shows a strong decrease from the center of the window at 2.03 μm to its wing at 2.12 μm, for all three locations. The mean decrease slope is -1.1 for the Huygens landing site, -1.106 for the dark area, and -1.33 for the bright one.

[44] The final step of this work is the retrieval of information on the nature of Titan's surface using our inferred surface albedo. Organics, H_2O ice, and CH_4 ice have been previously suggested as possible candidates for the surface constituents on Titan from both ground-based and Cassini-Huygens data [*Coustenis et al.*, 1995, 2006; *Griffith et al.*, 2003; *Tomasko et al.*, 2005; *Hartung et al.*, 2006; *Hirtzig et al.*, 2006, 2007]. Although a comparison with possible surface constituents should ideally be performed over a wider spectral range, we compared our 2-μm surface spectra with the spectra of tholins [*Coll et al.*, 1999], H_2O ice [*Grundy and Schmitt*, 1998], CH_4 ice [*Grundy et al.*, 2002], CO_2 ice [*Quirico and Schmitt*, 1997], and NH_3 ice [*Schmitt et al.*, 1998]. All these ice and tholin spectra are plotted in Figure 11 of *Negrão et al.* [2006]. From all of these, only the CH_4 ice spectra show a strong decreasing slope in the 2-μm region and could then be compatible with our data. The melting point of CH_4 ice is 91 K, very close to Titan's surface temperature of 94 K. Its presence on Titan's surface cannot thus be discarded. CH_4 ice is also compatible with the surface spectral behavior of the Xanadu region, appearing always bright in the windows at 1.28, 1.6 and 2.0 μm, consistent with the CH_4 ice spectral shape (see *Hirtzig et al.* [2006, 2007] for more details). However, the CH_4 ice albedo as reported from laboratory measurements, is quite high in this area. In order to dampen it, one could imagine the presence of organics (or tholin) mixed with the ice.

[45] DISR detected an absorption feature in the surface reflectivity at around 1.56 μm [*Tomasko et al.*, 2005, Figure 15b]. This is compatible with H_2O ice, which shows a strong absorption in this spectral region. However, we do not see in our surface albedo here any indication of the H_2O ice signature in particular, since we do not observe the increase beyond 2.1 μm. On the other hand, the H_2O ice spectral variation is not very strong between 2 and 2.1 μm, in the bottom of the absorption band [see *Negrão et al.*, 2006, Figure 11]. We should note however that, while DISR made its measurements at a very precise location on Titan's surface, our spatial resolution element concerns an area of about 175,000 km^2. This should be taken in consideration when doing comparisons with DISR observations.

[46] We thus believe that a mixture of H_2O ice, CH_4 ice and some dark component (tholins?) is compatible with the CFHT and VLT data, although we cannot propose here a specific mixture which could fit the two sets of observations

simultaneously. In all cases, we believe that our results can add constraints to more elaborate surface models and for the subsequent retrieval of Titan's surface constituents.

5. Discussion and Conclusions

[47] We have spectrally explored three different latitude areas on Titan's disk, one of which contains the landing site of the Huygens probe. We have modeled the recorded spectral regions (from 2.03 to 2.40 μm) and inferred information on the atmospheric characteristics and the surface properties.

[48] We find that the data in the methane band (for $\lambda >$ 2.2 μm) for the E and D areas can be fitted with similar vertical haze profiles down to about 90 km in altitude, whereas different behaviors below this altitude are required. For the bright area we found a smaller haze concentration than for the E and D areas at high altitudes. We find that by using a 5% of methane abundance at the surface (as determined by Huygens instruments [*Niemann et al.*, 2005; *Tomasko et al.*, 2005]), we produce quite good fits to our spectrum (between 2.12 and 2.2 μm, where our data are sensitive to this parameter). We find a total haze opacity at the equator and in the center of the 2-μm methane window compatible with the *Gibbard et al.* [2004] results as concerns the haze opacity variation at the equator as a function of the solar longitude.

[49] The line-by-line methane absorption coefficients calculations of *Boudon et al.* [2006] produce a good fit in the methane band, where the features of the data are only due to the atmospheric methane. The band model tested in this work [*Irwin et al.*, 2006] also yields a satisfactory fit in this spectral region.

[50] With respect to Titan's surface, we have studied a location encompassing the Huygens landing site (locus E). We have inferred its surface albedo, as well as that of neighboring areas (one among the brightest observed in our initial image and another dark one). We find the Huygens surface albedo at 2.03 μm to be close to 0.116. This value is compatible with the averaged surface albedo of 0.12 we have inferred for Titan's trailing hemisphere disk-averaged data taken in 1993 and 1994 at the CFHT [*Negrão et al.*, 2006]. *Griffith et al.* [2003] find surface albedos of about 0.1 at 2 μm for the trailing side of Titan. This is quite compatible with our values given the difference in spatial coverage and also in view of the uncertainties caused by the use of different methane absorption coefficients (we use the theoretical database of *Boudon et al.* [2006], giving different atmospheric transmissions at different altitude layers, while *Griffith et al.* [2003] have adopted a single value of 0.005 (km amagat)$^{-1}$ at 2 μm). Our values at the center of the window are somewhat higher than the *Gibbard et al.* [2004] values, who, by using speckle and adaptive optics images of Titan at 2 μm, found surface reflectivities of the order of 0.06 at longitudes of 200°W (see Gibbard et al.'s Figure 1). However, the values are compatible when the whole region of retrieval of the surface albedo is considered because (as discussed below) we find a strong decrease from one end to the other in the 2.03–2.115 μm region. Direct comparison with the recent Descent Imager/Spectral Radiometer (DISR) results [*Tomasko et al.*, 2005] cannot be made since the spectral range of the DISR instrument stops at 1.6 μm.

[51] Our brightest area in this hemisphere yields a surface albedo of about 0.14 at 2.03 μm, quite similar to our inferences from the CFHT data [*Negrão et al.*, 2006]. The value for Titan's disk-averaged leading side from the Griffith et al.'s measurements is 0.12. We then seem to be finding higher albedo values in our results in general, but given the uncertainties and the different geometries involved, we can only note the closeness of all these values and their intercompatibility.

[52] We found in this work the surface albedo to show a strong decrease from the center of the 2-μm window to its wing. The spectral shape of the surface albedo derived here is quite similar to the one found in the same spectral region (2 μm) and published by *Negrão et al.* [2006]. This is true in particular for the resulting surface albedo from the analysis of the disk-averaged data taken in 1993 and 1995 at the CFHT [*Negrão et al.*, 2006, Figure 10a] using the same code as here. In the cited work, the surface albedo also decreases roughly from 0.19 to 0.15 for the bright hemisphere and 0.15 to 0.12 for the darker side within the 2.03–2.11 μm region (slopes of −0.65 and −0.5, respectively). However, the decrease in the albedo in the VLT data is more pronounced than in the CFHT disk-averaged data. Nevertheless, the retrieved surface albedos for the bright region (locus R), both with the haze profile assumed in this work and with the haze obtained by *Negrão et al.* [2006], are within the error bars below around 2.08 μm (Figure 8). Above this wavelength the surface albedos diverge since the surface contribution to the total flux is smaller and thus the effect of a different haze profile is more noticeable.

[53] *Negrão et al.* [2006] interpreted the absorption-like spectral shape in the 2-μm window as a possible detection of H_2O ice, which was also observed by DISR at 1.6 μm [*Tomasko et al.*, 2005]. On the other hand, the surface albedo obtained in this work suggests the presence of CH_4 ice. However, these differences are in fact indicative of the sensitivity of our analysis on the haze vertical profile (as described in section 4.2). Indeed, the differences in the surface albedo shapes that we find beyond 2.06 μm, are mainly due to the different "cutoffs" or vertical distributions of the aerosols below a certain altitude. As shown in Figure 6, for the CFHT data we found a profile with a significant reduction of the aerosols below 110 km to better match the observations in the methane bands, whereas for the VLT data presented here we find a better agreement with the data when a profile with a constant haze opacity is used below roughly 90 km and to the ground (as discussed in section 4.1.2). When the CFHT haze vertical profile is used with the VLT data, the spectral behavior of the surface albedo in the 2.05–2.12 μm region changes from our nominal results and gives something similar to what was found in the *Negrão et al.* [2006, Figure 10a] analysis, namely, an increase in the long-wavelength part of the 2-μm methane window (Figure 8).

[54] Another parameter to consider and which could play a part in the lower VLT surface albedos found here is the presence of tropospheric clouds (which were not included in our atmospheric model) during our CFHT 1993 and 1995 observations. Such clouds were reported by *Griffith et al.*

[1998] in 1995 data at 1.6 and 2.0 μm. They were also reported in Titan's south pole in Cassini/VIMS observations in 2004 [*Porco et al.*, 2005], but found to have disappeared by 2005 [*Schaller et al.*, 2006], as confirmed by ground-based observations [*Coustenis et al.*, 2006; *Hirtzig et al.*, 2006, 2007]. (For a more detailed discussion about clouds on Titan, see also *Griffith et al.* [2005] and *Roe et al.* [2005].) The effect of such clouds, when not taken into account in our modeling, would be to artificially cause an increase in the disk-averaged "surface albedo" to compensate their absence. Since we have not included clouds in our model of the CFHT data, we have then possibly overestimated the surface albedos reported therein. In particular, for the trailing hemisphere of Titan (1993 data), this could explain the different surface albedo values between the CFHT and the VLT. The fact that the VLT data presented here were taken at a time when all observations agree as to the absence of clouds, renders the inferred surface albedos here all the more credible.

[55] In conclusion, the differences in shape and values between the surface albedos derived from the CFHT and the VLT data in the 2-μm window may be due to the differences in the haze profiles, the presence of clouds in the CFHT data or local changes in the surface composition (visible due to the difference in spatial resolution between the two data sets).

[56] The surface albedo shape that we find here was then compared with different ices and tholins spectra and showed to be compatible with the presence of CH_4 ice on Titan's surface. This ice, mixed with H_2O ice and tholins, could justify the VLT and CFHT retrieved surface albedos.

[57] The purpose of our study may become more obvious in the future when the Huygens probe's location results from the probe's instruments are used to extrapolate the composition of Titan's surface at other locations on the leading and trailing sides of Titan's disk.

[58] **Acknowledgments.** The data presented here are based on observations collected at the European Southern Observatory, Chile (ESO proposal 74.E-0747 with NACO). A. Negrão is supported by the FCT Ph.D. scholarship SFRH/BD/8006/2002.

References

Ádámkovics, M., I. de Pater, M. Hartung, F. Eisenhauer, R. Genzel, and C. A. Griffith (2006), Titan's bright spots: Multiband spectroscopic measurement of surface diversity and hazes, *J. Geophys. Res.*, *111*, E07S06, doi:10.1029/2005JE002610.

Barnes, J. W., et al. (2005), A 5-micron-bright spot on Titan: Evidence for surface diversity, *Science*, *310*, 92–95.

Boudon, V., M. Rey, and M. Loete (2006), The vibrational levels of methane obtained from analyses of high-resolution spectra, *J. Quant. Spectrosc.*, *98*, 394–404.

Brown, M. E., A. H. Bouchez, and C. A. Griffith (2002), Direct detection of variable tropospheric clouds near Titan's south pole, *Nature*, *420*, 795–797.

Caldwell, J., C. C. Cunningham, D. Anthony, H. P. White, E. J. Groth, H. Hasan, K. Noll, P. H. Smith, M. G. Tomasko, and H. A. Weaver (1992), Titan: Evidence for seasonal change—A comparison of Hubble Space Telescope and Voyager images, *Icarus*, *97*, 1–9.

Chanover, N. J., C. M. Anderson, C. P. McKay, P. Rannou, D. A. Glenar, J. J. Hillman, and W. E. Blass (2003), Probing Titan's lower atmosphere with acousto-optic tuning, *Icarus*, *163*, 150–163.

Coll, P., D. Coscia, N. Smith, M.-C. Gazeau, S. I. Ramirez, G. Cernogora, G. Israel, and F. Raulin (1999), Experimental laboratory simulation of Titan's atmosphere (aerosols and gas phase), *Planet. Space Sci.*, *47*, 1331–1340.

Coustenis, A., E. Lellouch, J.-P. Maillard, and C. P. McKay (1995), Titan's surface: Composition and variability from the near-infrared albedo, *Icarus*, *118*, 87–104.

Coustenis, A., E. Gendron, O. Lai, J.-P. Véran, J. Woillez, M. Combes, L. Vapillon, T. Fusco, L. Mugnier, and P. Rannou (2001), Images of Titan at 1.3 and 1.6 μm with adaptive optics at the CFHT, *Icarus*, *154*, 501–515.

Coustenis, A., M. Hirtzig, E. Gendron, P. Drossart, O. Lai, M. Combes, and A. Negrão (2005), Maps of Titan's surface from 1 to 2.5 μm, *Icarus*, *177*, 89–105.

Coustenis, A., A. Negrão, A. Salama, B. Schulz, E. Lellouch, P. Rannou, P. Drossart, T. Encrenaz, B. Schmitt, V. Boudon, and A. Nikitin (2006), Titan's 3-micron spectral region from ISO high-resolution spectroscopy, *Icarus*, *180*, 176–185.

Gendron, E., et al. (2004), VLT/NACO adaptive optics imaging of Titan, *Astron. Astrophys.*, *417*, L21–L24.

Gibbard, S. G., B. Macintosh, D. Gavel, C. E. Max, I. de Pater, A. M. Ghez, E. F. Young, and C. P. McKay (1999), Titan: High-resolution speckle images from the Keck Telescope, *Icarus*, *139*, 189–201.

Gibbard, S. G., I. de Pater, B. A. Macintosh, H. G. Roe, C. E. Max, E. F. Young, and C. P. McKay (2004), Titan's 2 μm surface albedo and haze optical depth in 1996–2004, *Geophys. Res. Lett.*, *31*, L17S02, doi:10.1029/2004GL019803.

Griffith, C. A., T. Owen, and R. Wagener (1991), Titan's surface and troposphere, investigated with ground-based, near-infared observations, *Icarus*, *93*, 362–378.

Griffith, C. A., T. Owen, G. A. Miller, and T. Geballe (1998), Transient clouds in Titan's lower atmosphere, *Nature*, *395*, 575–578.

Griffith, C. A., T. Owen, T. R. Geballe, J. Rayner, and P. Rannou (2003), Evidence for the exposure of water ice on Titan's Surface, *Science*, *300*, 628–630.

Griffith, C. A., et al. (2005), The evolution of Titan's mid-latitude clouds, *Science*, *310*, 474–477.

Grundy, W. M., and B. Schmitt (1998), The temperature-dependent near-infrared absorption spectrum of hexagonal H_2O ice, *J. Geophys. Res.*, *103*, 25,809–25,822.

Grundy, W., B. Schmitt, and E. Quirico (2002), The temperature-dependent spectrum of methane ice between 0.7 and 5 μm and opportunities for near-infrared remote thermometry, *Icarus*, *155*, 486–496.

Hartung, M., T. M. Herbst, C. Dumas, and A. Coustenis (2006), Limits to the abundance of surface CO_2 ice on Titan, *J. Geophys. Res.*, *111*, E07S09, doi:10.1029/2005JE002642.

Hilico, J. C., J. P. Champion, S. Toumi, V. G. Tyuterev, and S. A. Tashkun (1994), New analysis of the pentad system of methane and prediction of the (pentad-pentad) spectrum, *J. Molec. Spectrosc.*, *168*, 455–476.

Hirtzig, M., A. Coustenis, E. Gendron, P. Drossart, A. Negrão, M. Combes, O. Lai, P. Rannou, S. Lebonnois, and D. Luz (2006), Monitoring atmospheric phenomena on Titan, *Astron. Astrophys.*, *456*(2), 761–774.

Hirtzig, M., A. Coustenis, E. Gendron, P. Drossart, M. Hartung, A. Negrão, P. Rannou, and M. Combes (2007), Titan: Atmospheric and surface features as observed with Nasmyth Adaptive Optics System Near-Infrared Imager and Spectrograph at the time of the Huygens mission, *J. Geophys. Res.*, doi:10.1029/2005JE002650, in press.

Imanaka, H., B. N. Khare, J. E. Elsila, E. L. O. Bakes, C. P. McKay, D. P. Cruikshank, S. Sugita, T. Matsui, and R. N. Zare (2004), Laboratory experiments of Titan tholin formed in cold plasma at various pressures: Implications for nitrogen-containing polycyclic aromatic compounds in Titan haze, *Icarus*, *168*, 344–366.

Irwin, P. G. J., L. A. Sromovsky, E. K. Strong, K. Sihra, N. Bowles, S. B. Calcutt, and J. J. Remedios (2006), Improved near-infrared methane band models and k-distribution parameters from 2000 to 9500 cm^{-1} and implications for interpretation of outer planet spectra, *Icarus*, *181*, 309–319.

Khare, B. N., C. Sagan, E. T. Arakawa, F. Suits, T. A. Callcott, and M. W. Williams (1984), Optical constants of organic tholins produced in a simulated Titanian atmosphere—From soft X-ray to microwave frequencies, *Icarus*, *60*, 127–137.

Lellouch, E. (1990), Atmospheric models of Titan and Triton, *Ann. Geophys.*, *8*, 653–660.

Lellouch, E., A. Coustenis, D. Gautier, F. Raulin, N. Dubouloz, and C. Frere (1989), Titan's atmosphere and hypothesized ocean—A reanalysis of the Voyager 1 radio-occultation and IRIS 7.7-micron data, *Icarus*, *79*, 328–349.

Lellouch, E., B. Schmitt, A. Coustenis, and J.-G. Cuby (2004), Titan's 5-micron lightcurve, *Icarus*, *168*, 209–214.

Lemmon, M. T., E. Karkoschka, and M. Tomasko (1995), Titan's rotational light-curve, *Icarus*, *113*, 27–38.

Letourneur, B., and A. Coustenis (1993), Titan's atmospheric structure from Voyager 2 infrared spectra, *Planet. Space Sci.*, *41*, 593–602.

Lockwood, G. W., B. L. Lutz, D. T. Thompson, and E. S. Bus (1986), The albedo of Titan, *Astrophys. J.*, *303*, 511–520.

Lorenz, R. D., P. H. Smith, M. T. Lemmon, E. Karkoschka, G. W. Lockwood, and J. Caldwell (1997), Titan's north-south asymmetry from HST and Voyager imaging: Comparison with models and ground-based photometry, *Icarus*, *127*, 173–189.

Lorenz, R. D., M. T. Lemmon, P. H. Smith, and G. W. Lockwood (1999), Seasonal change on Titan observed with the Hubble Space Telescope WFPC-2, *Icarus*, *142*, 391–401.

Lorenz, R. D., E. F. Young, and M. T. Lemmon (2001), Titan's smile and collar: HST observations of seasonal change 1994–2000, *Geophys. Res. Lett.*, *28*, 4453–4456.

McKay, C. P., J. B. Pollack, and R. Courtin (1989), The thermal structure of Titan's atmosphere, *Icarus*, *80*, 23–53.

Negrão, A., A. Coustenis, E. Lellouch, J.-P. Maillard, P. Rannou, B. Schmitt, C. P. McKay, and V. Boudon (2006), Titan's surface albedo variations over a Titan season from near-infrared CFHT/FTS spectra, *Planet. Space Sci.*, *54*, 1225–1246.

Niemann, H. B., et al. (2005), The abundances of constituents of Titan's atmosphere from the GCMS instrument on the Huygens probe, *Nature*, *438*, 779–784.

Perryman, M. A. C., et al. (1997), The HIPPARCOS Catalogue, *Astron. Astrophys.*, *323*, L49–L52.

Pollack, J. B., and C. P. McKay (1985), The impact of polar stratospheric clouds on the heating rates of the winter polar stratosphere, *J. Atmos. Sci.*, *42*, 245–262.

Porco, C. C., et al. (2005), Imaging of Titan from the Cassini spacecraft, *Nature*, *434*, 159–168.

Quirico, E., and B. Schmitt (1997), Near-infrared spectroscopy of simple hydrocarbons and carbon oxides diluted in solid N_2 and as pure ices: Implications for Triton and Pluto, *Icarus*, *127*, 354–378.

Rannou, P., C. P. McKay, and R. D. Lorenz (2003), A model of Titan's haze of fractal aerosols constrained by multiple observations, *Planet. Space Sci.*, *51*, 963–976.

Roe, H. G., I. de Pater, B. A. Macintosh, and C. P. McKay (2002), Titan's clouds from Gemini and Keck adaptive optics imaging, *Astrophys. J.*, *581*, 1399–1406.

Roe, H. G., M. E. Brown, E. L. Schaller, A. H. Bouchez, and C. A. Trujillo (2005), Geographic control of Titan's mid-latitude clouds, *Science*, *310*, 477–479.

Rousset, G., et al. (2003), NAOS, the first AO system of the VLT: On-sky performance, in *Adaptive Optical System Technologies II*, edited by P. L. Wizinowich and D. Bonaccini, *Proc. SPIE*, *4839*, 140–149.

Schaller, E. L., M. E. Brown, H. G. Roe, and A. H. Bouchez (2006), A large cloud outburst at Titan's south pole, *Icarus*, *182*, 224–229.

Schmitt, B., E. Quirico, F. Trotta, and W. Grundy (1998), Optical properties of ices from UV to infrared, in *Solar System Ices*, *Astrophys. Space Sci. Lib.*, vol. 227, edited by B. Schmitt, C. de Bergh, and M. Festou, pp. 199–240, Springer, New York.

Smith, B. A., et al. (1981), Encounter with Saturn—Voyager 1 imaging science results, *Science*, *212*, 163–191.

Smith, B. A., et al. (1982), A new look at the Saturn system: The Voyager 2 images, *Science*, *215*, 505–537.

Smith, P. H., M. T. Lemmon, R. D. Lorenz, L. A. Sromovsky, J. J. Caldwell, and M. D. Allison (1996), Titan's surface, revealed by HST imaging, *Icarus*, *119*, 336–349.

Sromovsky, L. A., V. E. Suomi, J. B. Pollack, R. J. Krauss, S. S. Limaye, T. Owen, H. E. Revercomb, and C. Sagan (1981), Implications of Titan's north-south brightness asymmetry, *Nature*, *292*, 698–702.

Tomasko, M. G., et al. (2005), Rain, winds and haze during the Huygens probe's descent to Titan's surface, *Nature*, *438*, 765–778.

Tran, T.-T., and P. Rannou (2004), Comparing 3D spherical Monte-Carlo and 2-stream parallel plane simulation of far-field backscattering image of Titan, *Notes Pole Planet. Inst. Pierre Simon Laplace*, *2*.

Wenger, C., and J.-P. Champion, (1998) Spherical Top Data System (STDS) software for the simulation of spherical top spectra, *J. Quant. Spectrosc. Radiat. Transfer*, *59*, 471–480.

Young, E. F., P. Rannou, C. P. McKay, C. A. Griffith, and K. Noll (2002), A three-dimensional map of Titan's tropospheric haze distribution based on Hubble Space Telescope imaging, *Astron. J.*, *123*, 3473–3486.

V. Boudon, Laboratoire de Physique de l'Université de Bourgogne, CNRS UMR 5027, 9, Avenue Alain Savary, B.P. 47 870, F-21078 Dijon Cedex, France.

A. Coustenis, M. Combes, P. Drossart, and E. Gendron, LESIA, Observatoire de Paris-Meudon, F-92195 Meudon Cedex, France.

M. Hirtzig, Laboratoire de Planétologie et de Géodynamique Faculté des Sciences, 2 rue de la Houssinière BP 92 208, F-44322 Nantes Cedex 03, France.

A. Negrão, Laboratoire d'Etudes Spatiales et d'Instrumentation en Astrophysique Observatoire de Paris - Section de Meudon, 5 Place Jules Janssen, F-92195 MEUDON Cedex, France. (alberto.negrao@obspm.fr)

P. Rannou, Service d'Aéronomie, Institut Pierre Simon Laplace, Université de Versailles Saint-Quentin-en-Yvelines, Verrières le Buisson, France.